Hydrodynamic interactions induce anomalous diffusion under partial confinement
Supplementary Information

February 11, 2014

Sections 1–3 give an extended discussion of the Theory section of the main paper, i.e. on the hydrodynamic model and its consequences for the diffusion coefficient. The case of an ideal gas is discussed in detail since it is partially amenable to an analytical treatment. Section 4 summarizes the main relations of a dynamical model for gravitating particles trapped at fluid interfaces (gas of capillary monopoles) which has been developed by the authors in previous years. Section 5 presents more details on the simulations, with an emphasis on the discussion of fixing parameters in the Lattice–Boltzmann simulations.

1 The hydrodynamic model

The hydrodynamic model described by Eqs. (2-4) is based on the so-called Faxén law [1] for the motion of a sphere in a fluid at low Reynolds number[1]: if a rigid sphere of radius a moves with velocity $\mathbf{v}$ under the action of an external force $\mathbf{f}$ while immersed in an ambient Stokes flow $\mathbf{u}(\mathbf{r})$ (which is induced by sources outside of the particle), then it holds exactly

$$\mathbf{v} = \Gamma\mathbf{f} + \left(1 + \frac{a^2}{6}\nabla^2\right)\mathbf{u}(\mathbf{r}_c), \tag{1.A}$$

with $\Gamma = 1/(6\pi\eta a)$ and $\mathbf{r}_c :=$ position of sphere center. The effect of the hydrodynamic interactions is modeled by an effective ambient flow field $\mathbf{u}(\mathbf{r})$ determined by the rest of the particles in the system. We employ a mean–field–like approximation by which it is assumed that this field is smooth on the microscopic scale (and thus the term $a^2\nabla^2\mathbf{u}$ in Eq. (1.A) is negligible, giving Eq. (3)), and $\mathbf{u}(\mathbf{r})$ is determined self–consistently as a functional solely of a *smooth* density field $\rho(\mathbf{r})$, thus neglecting explicit account of interparticle correlations. The simplest approximation for this functional dependence is obtained when the effective ambient flow represents a Stokes flow induced by the forces driving the particles, i.e.,

$$\eta\nabla^2\mathbf{u} - \nabla p = -\rho(\mathbf{r})\mathbf{f}(\mathbf{r}), \qquad \nabla\cdot\mathbf{u} = 0, \tag{1.B}$$

where p is the pressure field enforcing the incompressibility constraint. This equation is complemented with the boundary condition that the ambient flow field is absolutely integrable, in which case the solution is given by Eq. (4) in terms of the Oseen tensor, which is the Green function for our boundary value problem. That is, only the force monopole of the particles is retained explicitly for computing the hydrodynamic interactions because it provides the source of the dominant far–field contribution [1]. This approximation deserves several remarks:

- The proposed boundary value problem has a solution only if the total external force acting on the system vanishes,

$$\int d^3\mathbf{r}\,\rho(\mathbf{r})\mathbf{f}(\mathbf{r}) = 0. \tag{1.C}$$

  This is the case for a thermodynamic generalized force due to particle–particle interactions (by the principle of action–reaction) or to thermal motion when the density field is homogeneous at infinity (because $\rho\mathbf{f}_{\text{thermal}} \propto \nabla\rho$). The effect of a net force has to be accounted for by means of an ambient flow that does not vanish at infinity (for instance, the so-called "backflow" in the problem of sedimentation under the action of gravity, see, e.g., Refs. [2, 3]).

[1] The restriction to a sphere is made for simplicity. The basic idea of the approximation can be applied for arbitrarily shaped rigid particles by the corresponding generalization of the Faxén law.

- If the thermodynamic generalized force can be derived from a free energy functional $\mathcal{F}[\rho]$,

$$\mathbf{f}(\mathbf{r}) = -\nabla \frac{\delta \mathcal{F}}{\delta \rho(\mathbf{r})}, \tag{1.D}$$

  Equations (2–4) become a simple version of the dynamic density functional theory extended to include hydrodynamic interactions as presented recently in Ref. [4] (the model presented in that work incorporates the effect of hydrodynamic interactions at the Rotne–Prager level, rather than at the simpler Oseen level, as in our model).

- The mean–field–like approximation embodied in Eq. (1.B) can be justified easily in the dilute limit, when interparticle correlations are weak anyhow. Beyond this limit, the approximation also holds actually in the "macroscopic regime" of small gradients valid to address the large–scale, long–time evolution, provided Γ and η are interpreted as effective, possibly density–dependent rheological coefficients different from their bare (dilute–limit) values (see Refs. [5, 6]).

2 The diffusion coefficient

The 2D Fourier transform of the density is defined as

$$\delta\rho_{\mathbf{k}} = \int d^2\mathbf{r}\, \mathrm{e}^{-i\mathbf{k}\cdot\mathbf{r}} \delta\rho(\mathbf{r}), \quad \delta\rho(\mathbf{r}) = \int \frac{d^2\mathbf{k}}{(2\pi)^2}\, \mathrm{e}^{i\mathbf{k}\cdot\mathbf{r}} \delta\rho_{\mathbf{k}}, \tag{2.A}$$

and similarly for the other fields, whereby $\mathbf{k}$ is a vector in the reciprocal 2D space. Equation (5) can be written now as

$$\frac{\partial \delta\rho_{\mathbf{k}}}{\partial t} \approx \rho_{\mathrm{hom}}\, i\mathbf{k} \cdot [\Gamma \mathbf{f}_{\mathbf{k}} + \mathbf{u}_{\mathbf{k}}], \tag{2.B}$$

whereas the convolution in Eq. (4) is written after linearization as

$$\mathbf{u}_{\mathbf{k}} \approx \frac{\rho_{\mathrm{hom}}}{8\pi\eta} \mathbf{f}_{\mathbf{k}} \cdot \int d^2\mathbf{x}\, \mathrm{e}^{-i\mathbf{k}\cdot\mathbf{x}} \mathcal{G}(\mathbf{x}). \tag{2.C}$$

Combination of Eqs. (2.B,2.C) gives (in component form)

$$\frac{\partial \delta\rho_{\mathbf{k}}}{\partial t} \approx \Gamma \rho_{\mathrm{hom}} \sum_{\alpha,\beta=1}^{2} ik_\alpha (\mathbf{f}_{\mathbf{k}})_\beta \left[\delta_{\alpha\beta} + \frac{\rho_{\mathrm{hom}}}{8\pi\eta\Gamma} \int d^2\mathbf{x}\, \mathrm{e}^{-i\mathbf{k}\cdot\mathbf{x}} \mathcal{G}_{\alpha\beta}(\mathbf{x}) \right]. \tag{2.D}$$

In the absence of hydrodynamic interactions, the dynamics of the system is assumed diffusive, so that consistently with the "large–scale, long–time" nature of the model, the (perturbation in the) force is proportional to the density gradient,

$$\mathbf{f}_{\mathbf{k}} \approx \frac{D_0(k)}{\rho_{\mathrm{hom}}\Gamma} (-i\mathbf{k}) \delta\rho_{\mathbf{k}}, \tag{2.E}$$

with a proportionality coefficient $D_0(k)$ that represents the wave number dependent diffusion coefficient in the absence of hydrodynamic interactions. When Eq. (2.E) is inserted in Eq. (2.D), the latter becomes Eq. (1) with a diffusion coefficient

$$D(k) = [1 + g(k)] D_0(k), \tag{2.F}$$

and $g(k)$ given by Eq. (6). The function $g(k)$ can be most easily computed by introducing the 3D Fourier transform of the Oseen tensor [1],

$$\mathcal{G}_{\alpha\beta}(\mathbf{x}) = \int \frac{d^3\mathbf{q}}{(2\pi)^3} \mathrm{e}^{i\mathbf{q}\cdot\mathbf{x}} \frac{8\pi}{q^2} \left[\delta_{\alpha\beta} - \frac{q_\alpha q_\beta}{q^2} \right], \tag{2.G}$$

with the 3D reciprocal vector $\mathbf{q} = (\mathbf{q}_\parallel, q_z)$, in terms of the 2D projection $\mathbf{q}_\parallel$ and the vertical component q_z. Since $\mathbf{x}$ represents a position in the plane $z = 0$, one has $\mathbf{q}\cdot\mathbf{x} = \mathbf{q}_\parallel \cdot \mathbf{x}$, and when Eq. (2.G) is inserted in the definition (6) the integral over $\mathbf{x}$ evaluates to a 2D Dirac delta $\delta(\mathbf{k} - \mathbf{q}_\parallel)$, so that

$$\begin{aligned} g(k) &= \frac{1}{2\pi L_{\mathrm{hydro}}} \sum_{\alpha,\beta} \frac{k_\alpha k_\beta}{k^2} \int_{-\infty}^{+\infty} \frac{dq_z}{2\pi} \frac{8\pi}{k^2 + q_z^2} \left[\delta_{\alpha\beta} - \frac{k_\alpha k_\beta}{k^2 + q_z^2} \right] \\ &= \frac{2}{\pi L_{\mathrm{hydro}}} \int_{-\infty}^{+\infty} dq_z\, \frac{q_z^2}{(k^2 + q_z^2)^2} = \frac{1}{k L_{\mathrm{hydro}}}. \end{aligned} \tag{2.H}$$

As remarked in the manuscript, the notion of partial confinement also applies when the particles are restricted to move on a line. The previous calculations still apply, except that the function $g(k)$ is now expressed in terms of the 1D Fourier transform of the 3D Oseen tensor, namely,

$$g(k) = \frac{\rho_{\rm hom}}{8\pi\eta\Gamma}\int_{-\infty}^{+\infty} dx\, {\rm e}^{-ikx}\mathcal{G}_{11}(x), \tag{2.I}$$

assuming the line of confinement is parameterized as $y=0, z=0$. From Eq. (4) one sees that $\mathcal{G}_{11}(x) = 2/|x|$, so that

$$g(k) = \frac{2}{\pi L_{\rm hydro}}\int_0^{\infty} dx\, \frac{\cos kx}{x}. \tag{2.J}$$

This integral is divergent at the lower limit, signaling that our simple mean–field approximation must be improved. For the purpose of addressing the large–scale features of the dynamics, one can introduce a small–scale cutoff, $x > \sigma$ (the particle size, for instance), and study the limit $k\sigma \to 0$. In such case, the result (2.J) is expressed in terms of the cosine integral function, with the asymptotic behavior [7]

$$g(k) \sim -\frac{2}{\pi L_{\rm hydro}}\ln k\sigma \qquad (k\sigma \to 0), \tag{2.K}$$

thus leading to anomalous diffusion in Eq. (2.F) again.

3 The ideal gas

For an ideal gas, the particles are driven only by Brownian motion and Eq. (2.E) holds with $D_0(k) = \Gamma k_B T$, so that Eq. (1) becomes

$$\frac{\partial \delta\rho_{\mathbf{k}}}{\partial t} = -D_0\,[1+g(k)]\,k^2\delta\rho_{\mathbf{k}}. \tag{3.A}$$

The associated linear equation for the real–space density field $\delta\rho(\mathbf{r},t)$ can be solved with the initial condition

$$\delta\rho(\mathbf{r},t=0) = \delta(\mathbf{r}) \quad \Leftrightarrow \quad \delta\rho(\mathbf{k},t=0) = 1, \tag{3.B}$$

and the boundary condition that $\delta\rho(\mathbf{r},t)$ is absolutely integrable (so that $\delta\rho_{\mathbf{k}}(t)$ exists). The solution is the so-called Green function, $G(\mathbf{r},t)$, of the problem, which can be easily obtained from Eq. (3.A),

$$\begin{aligned} G(\mathbf{r},t) &= \int \frac{d^2\mathbf{k}}{(2\pi)^2}\, {\rm e}^{i\mathbf{k}\cdot\mathbf{r}}{\rm e}^{-D_0[1+g(k)]k^2 t} \\ &= \frac{1}{D_0 t}\int \frac{d^2\mathbf{q}}{(2\pi)^2}\, {\rm e}^{\frac{i\mathbf{q}\cdot\mathbf{r}}{\sqrt{D_0 t}}}{\rm e}^{-(q^2+q\sqrt{t/t_{\rm hydro}})}, \end{aligned} \tag{3.C}$$

after inserting the form of $g(k)$, see Eq. (6), in terms of the time scale and the transformed integration variable

$$t_{\rm hydro} := \frac{L_{\rm hydro}^2}{D_0} \quad \text{and} \quad \mathbf{q} := \mathbf{k}\sqrt{D_0 t}, \tag{3.D}$$

respectively. Although this integral cannot be computed analytically, one can study its asymptotic behavior in two different limits:

- For times $t \ll t_{\rm hydro}$, one can neglect the term involving $t_{\rm hydro}$ in Eq. (3.C) because it is relevant only for an ever narrower range, $0 < q \lesssim \sqrt{t/t_{\rm hydro}}$, of the integration domain, so that $G(\mathbf{r},t)$ describes normal 2D diffusion,

$$G(r,t) \approx \frac{1}{4\pi D_0 t}{\rm e}^{-r^2/(4D_0 t)}. \tag{3.E}$$

- One can also write

$$G(\mathbf{r},t) = \frac{1}{L_{\rm hydro}^2}\int \frac{d^2\mathbf{p}}{(2\pi)^2}\, \mathrm{e}^{\frac{i\mathbf{p}\cdot\mathbf{r}}{L_{\rm hydro}}}\mathrm{e}^{-(p^2+p)(t/t_{\rm hydro})}, \tag{3.F}$$

in terms of the new integration variable $\mathbf{p} = \mathbf{q}/\sqrt{t/t_{\rm hydro}}$. In the limit $t \gg t_{\rm hydro}$, the integral is exponentially dominated by the values of p close to zero, so that one approximates

$$G(r,t) \approx \frac{1}{2\pi L_{\rm hydro}^2}\int_0^\infty dp\; pJ_0\left(\frac{pr}{L_{\rm hydro}}\right)\mathrm{e}^{-pt/t_{\rm hydro}}. \tag{3.G}$$

in terms of the Bessel function J_0 after performing the angular integration. This integral can be evaluated analytically [7] and is given in Eq. (7).

Fig. 3 illustrates the ideal gas evolution with and without hydrodynamic interactions, with the purpose of observing also the algebraic decay of the particle distribution profile predicted by Eq. (7).

4 The gas of capillary monopoles

A recent review of our latest work on this topic can be found in Ref. [8]. Here we summarize the most relevant aspects for the present work. A colloidal monolayer can be formed when the colloidal particles are trapped at a fluid interface. This creates an interfacial deformation that induces capillary forces between the particles. In the (experimentally relevant) case of small interfacial deformations, the capillary forces can be described via a multipolar expansion [9, 10], whereby the dominant contribution at large separations is the isotropic, monopolar term. The *capillary monopole* c_0 of a particle at the interface is given by the external force on the particle normal to the interface (e.g., the buoyant weight of the particles). The capillary potential energy between two such monopoles a distance x apart in the interface has the form

$$\phi(x) = -\frac{c_0^2}{2\pi\gamma}K_0\left(\frac{x}{\lambda}\right), \tag{4.A}$$

where γ is the surface tension of the interface, λ its capillary length, and K_0 a modified Bessel function. The potential decays exponentially at separations $x \gg \lambda$, but only logarithmically for $x \ll \lambda$ (like 2D Newtonian gravity). In many experimental configurations, $c_0 \neq 0$ and the resulting capillary attraction is very strong; additionally, $\lambda \sim$ mm while the interparticle separation is $\sim \mu$m, so that the net capillary force on a given particle results from the interaction with a large number of neighbors. As a consequence, a mean–field approximation is reliable. Concerning the large–scale dynamics, one can thus separate a generalized force $\mathbf{f}(\mathbf{r})$ at a point $\mathbf{r}$ on the interface into a local contribution and a nonlocal, mean–field capillary contribution [11],

$$\mathbf{f}(\mathbf{r}) = -\frac{1}{\rho(\mathbf{r})}\nabla p - \nabla V_{\rm cap}. \tag{4.B}$$

Here, $p(\rho(\mathbf{r}))$ is the (local) pressure of the 2D gas due to sources other than capillary attraction (Brownian motion, hard–core or electrostatic repulsion,...) and

$$V_{\rm cap}(\mathbf{r}) = \int d^2\mathbf{r}'\,\rho(\mathbf{r}')\phi\left(|\mathbf{r}-\mathbf{r}'|\right) \tag{4.C}$$

is the capillary potential energy of one particle due to the 2D gas (incidentally, the quantity $-V_{\rm cap}(\mathbf{r})/c_0$ is the vertical deformation of the fluid interface at the point $\mathbf{r}$). Upon expanding $\mathbf{f}$ in small density fluctuations $\delta\rho_{\mathbf{k}}$ about the homogeneous 2D density $\rho_{\rm hom}$ and using Eq. (2.E), one obtains $D_0(k)$ given by Eq. (8) with the characteristic time

$$\mathcal{T} = \frac{\gamma}{\Gamma c_0^2\rho_{\rm hom}}, \tag{4.D}$$

and the characteristic length

$$\mathcal{K}^{-1} = \sqrt{\frac{\gamma p'(\rho_{\rm hom})}{c_0^2\rho_{\rm hom}}}. \tag{4.E}$$

In addition to the explicit dependence on the physical parameters, the values of these scales are also controlled by the temperature, implicit in the pressure p. Ref. [11] studies in detail the ranges of variation of the values of $\mathcal{T}$ and $\mathcal{K}$ for various experimental setups with particles trapped at fluid interfaces which realize a fluid of capillary monopoles. As an example, a collection of hard spheres of radius $a = 10\,\mu$m whose capillary monopole is due to the buoyant weight typically has $\mathcal{K}^{-1} \approx 16\,\mu$m, $\mathcal{T} \approx 1500$ s at densities corresponding to a mean interparticle separation $\approx 3a$. Figure S1 shows the different qualitative shapes, dependent on the capillary length λ, of the growth rate $-k^2 D_0(k)$ as a function of the wave number k as predicted by Eqs. (1,8). A homogeneous particle distribution is unstable against clustering when $\lambda\mathcal{K} > 1$, which is achieved easily in typical experimental conditions [11]. Fig. 1 illustrates how the hydrodynamic interactions affect this linear evolution.

Beyond the linearized approximation valid only for small deviations from homogeneity, one can study analytically the limiting case $p \to 0$ (i.e., the only driving force is capillary attraction) and $\lambda \to \infty$ (i.e., the capillary attraction has an infinite range, like the Newtonian gravitational force). This scenario is dubbed "cold collapse" in the cosmological literature because $p = 0$ is interpreted as the zero temperature limit. In the linear regime, Eq. (8) reduces to $D_0(k) \to -(k^2\mathcal{T})^{-1}$, so that any density perturbation grows with the same rate $-1/(k^2 D_0) = \mathcal{T}$, see Eq. (1). The fully nonlinear regime is described by Eqs. (2–3, 4.B, 4.C) with $p = 0$, $\lambda \to \infty$ ("cold collapse") and $\mathbf{u} = 0$ (no hydrodynamic interactions), i.e.,

$$\frac{\partial \rho}{\partial t} = \Gamma \nabla \cdot (\rho \nabla V_{\rm cap}). \tag{4.F}$$

This equation can be solved analytically for radially symmetric configurations [11]. In particular, for an initial top–hat shape of radius R and density ρ_0 of the density profile, it is found that this shape remains undeformed and all the particles collapse simultaneously at the center after a time $\mathcal{T}$,

$$\rho(\mathbf{r},t) = \begin{cases} \dfrac{\rho_0}{\ell^2(t)}, & |\mathbf{r}| < R\ell(t) \\ 0, & R\ell(t) < |\mathbf{r}| \end{cases} \qquad \ell(t) = \sqrt{1 - \frac{t}{\mathcal{T}}}, \tag{4.G}$$

where the time $\mathcal{T}$ is defined by Eq. (4.D) after identifying $\rho_{\rm hom}$ with the initial value ρ_0 of the density inside the disk. When the assumption $\lambda \to \infty$ is relaxed, the problem can be studied perturbatively in $1/\lambda$ and one finds that the initial top–hat shape is deformed by the formation of a density peak at the outer rim of the disk [13, 14]. Fig. 2 shows the influence of the hydrodynamic interactions on this nonlinear evolution, both for $\lambda \to \infty$ and $\lambda < \infty$.

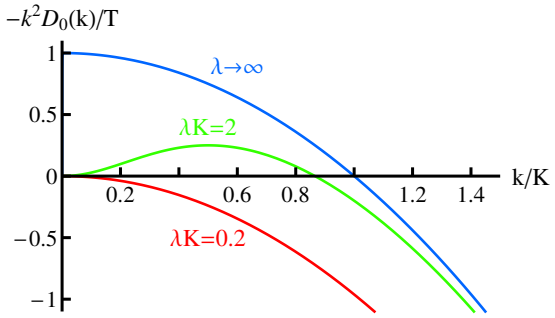

Figure S1 The theoretically predicted growth rate $-k^2 D_0(k)$ for the modes of density perturbations of a gas of capillary monopoles in the absence of hydrodynamic interactions. The growth rate is given in units of the characteristic time $\mathcal{T}$, the lengths are expressed in units of the characteristic length $\mathcal{K}^{-1}$.

5 Simulation setup

5.1 Brownian dynamics and truncated Stokesian dynamics

The 2D Brownian Dynamics (BD) simulations for the bulk and for a collapsing disk of capillary monopoles is described in detail in Refs. [12, 13]. The truncated Stokesian Dynamics (tSD) simulations incorporate the hydrodynamic interactions on the two–particle level by means of the Rotne–Prager tensor. We follow the standard procedure described, e.g., in Ref. [15]. Overdamped

motion of N hard spheres (radius a) with hydrodynamic interactions incorporated leads to individual particle velocities according to

$$\mathbf{v}_i = \frac{1}{k_B T} \sum_{j=1}^{N} \mathcal{D}(\mathbf{r}_i - \mathbf{r}_j) \cdot \mathbf{F}_j + \mathbf{s}_i, \tag{5.A}$$

where $\mathcal{D}$ denotes the Rotne–Prager tensor [16], given in terms of the Oseen tensor as

$$\mathcal{D}(\mathbf{r}) = \begin{cases} \dfrac{k_B T}{6\pi\eta a} I, & |\mathbf{r}| = 0, \\ \dfrac{k_B T}{8\pi\eta} \left[1 + \dfrac{1}{3} a^2 \nabla^2 \right] \mathcal{G}(\mathbf{r}), & |\mathbf{r}| \neq 0, \end{cases} \tag{5.B}$$

$\mathbf{s}_i(t)$ is a Gaussian noise with zero mean and variance

$$\langle \mathbf{s}_i(t) \mathbf{s}_j(t') \rangle = 2\mathcal{D}(\mathbf{r}_i - \mathbf{r}_j)\delta(t - t'), \tag{5.C}$$

and $\mathbf{F}_j$ is the force acting on the particle j, that includes the interaction with other particles and the force in the z–direction constraining the particles to stay in the plane $z = 0$. In principle it is wrong to sidestep the explicit use of a constraining force by the procedure of reducing the 3D dynamical equation (5.A) to its projection on the plane $z = 0$, because the stochastic dynamics described by this equation is correct only provided [15] $\nabla \cdot \mathcal{D} = 0$, which is true in 3D but not in 2D. This approximation would fail to capture correctly the contribution of the thermal motion to the induced ambient flow, making for instance that the Boltzmann–Gibbs distribution would not be a stationary solution of the associated Fokker–Planck equation. In practice, we find nonetheless that this approximation introduces no observable error in the simulated dynamics of a gas of capillary monopoles, because the effect of thermal motion is quantitatively negligible on the regimes of dynamical evolution studied. However, in an ideal gas, the dynamics is driving solely by thermal motion and both the Brownian motion in the z–direction and the constraining force have to be accounted for explicitly in Eq. (5.A). In such case, the constraining force was modelled with the confining potential

$$V_{\text{conf}}(z) = \left(\frac{2z}{a} \right)^2 k_B T. \tag{5.D}$$

Results do not depend on the specific form of $V_{\text{conf}}(z)$ as long as the lateral scale one considers is large compared to the width of the potential.

5.2 Lattice Boltzmann simulations

We used a combined 3D multi–component Lattice Boltzmann and Molecular dynamics simulation method (LB) [17, 18]. We configure the system such that the particles are trapped at an interface between two immiscible fluids. See the upper panel of Fig. S2 for an example configuration with only two particles. By applying a constant force perpendicular to the interface, it is deformed and capillary interactions come into play.

For a practical diffuse interface Lattice–Boltzmann simulation, it is impossible to simulate μm–sized particles at a sharp interface with a width of 1 nm. The interface widths will be around 3-5 lattice units, whereas particle sizes can be chosen a few times the interface width if one aims at simulating with about 50 particles. The strategy we therefore adopted is to demand that the nanoscopic Lattice–Boltzmann particles essentially obey overdamped dynamics: we require that the ratio of the velocity relaxation time τ_v to the characteristic time $\mathcal{T}$ of the capillary collapse (see Eq. (4.D)) is the same for both the tSD simulations and the LB simulations. In that way, the physical assumptions about the dynamical evolution among all approaches (mean–field theory, tSD and LB simulations) are the same. In detail, the setup was as follows.

We simulate a system of $L_x \times L_y \times L_z = 256 \times 256 \times 64$ lattice sites, occupied by two fluids and separated by an interface parallel to the x-y–plane. The initial majority and minority number densities of the fluid phases were set to 0.7 and 0.04 in lattice units, respectively. Both mass densities were kept fixed at unity and the kinematic viscosities were kept at $\nu = 1/6$. The particles were placed at the interface and after a few (~ 2000) equilibration timesteps, a force c_0 perpendicular to the interface acting only on the particles was applied. The resulting deformation of the interface gives rise to a monopolar capillary interaction given by Eq. (4.A), with the surface tension γ of the interface being determined by the fluid-fluid coupling constant g_{br} of the two fluids in the underlying Shan-Chen multi–component LB model. Here we use $g_{br} = 0.10$, which results in $\gamma = 0.0416$ in lattice

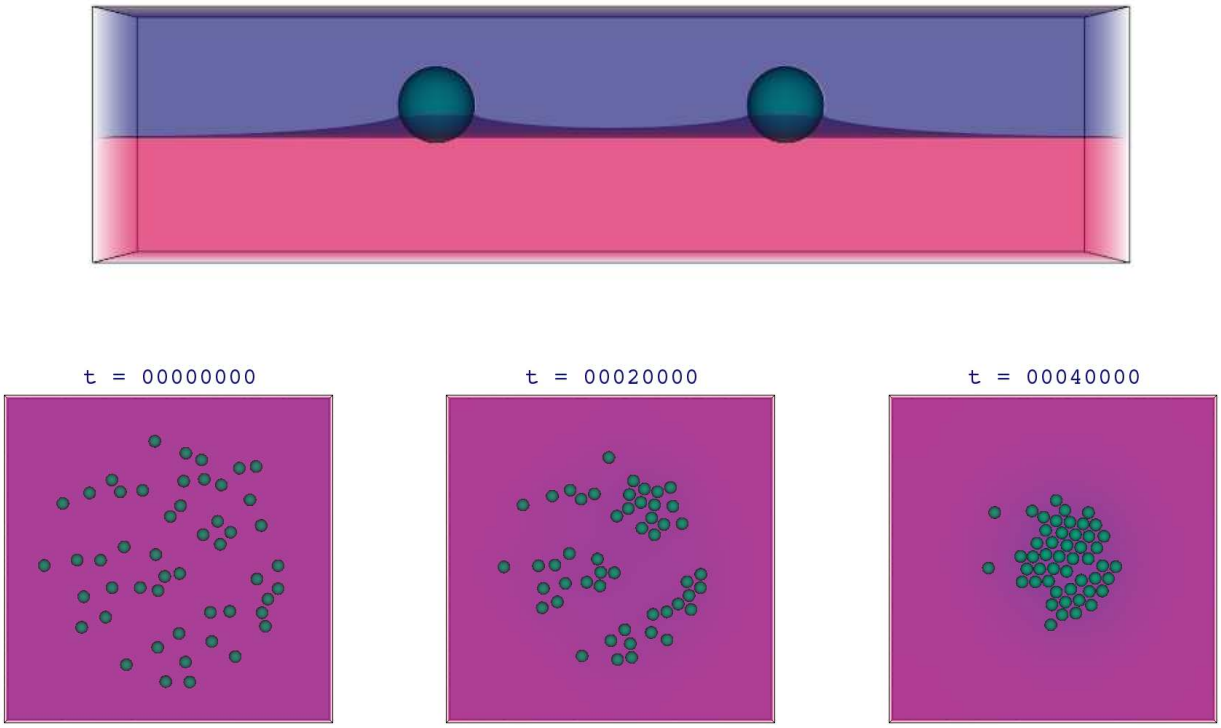

Figure S2 (Upper panel) Two particles trapped at a fluid interface between two immiscible fluids. The interface is deformed due to a constant force acting on the particles in positive z-direction. (Lower panel) Snapshots of the collapse of a disk–like distribution of $N = 50$ particles trapped at the fluid interface ($\rho_p = 1.76$, $c_0 = -0.08$, $\mathcal{T} = 44900$, other parameters as given in the text.)

units [17, 18]). After fixing the radius of the particles ($a = 5$ lattice units), their mass still remains as a free variable. We use the physical condition (mentioned above) of $\tau_v/\mathcal{T}$ being equal for tSD and LB. We have $\tau_v = m\Gamma$, and for the parameters given for Fig. 2 (see below), tSD gives $\tau_v/\mathcal{T} \approx 1.87 \times 10^{-3}$. We therefore choose a relative mass density of the particles as $\rho_p = 7.06$. Even with this constraint on the ratio $\tau_v/\mathcal{T}$ and thus the particle mass, different characteristic times may be achieved by varying the particle density and the applied force simultaneously (see Eq. (4.D)). We have therefore checked an alternative setup for these parameters ($\rho_p = 1.76$, $c_0 = -0.08$) and found the same dynamics (see also lower panel in Fig. S2).

With this choice of parameters, the mobility is given by $\Gamma = 10/(7\pi a)$ where we used the fact that the kinematic viscosity in the model is $\nu = 1/6$. The characteristic time (in lattice units) is $\mathcal{T} \approx 179600$ (see Eq. (4.D)).

5.3 Parameter values for Figs. (1–3)

Here we collect the specific values of the parameters employed in the different simulations leading to Figs. (1–3).

- Fig. 1 includes the results from tSD simulations of a collection of $N = 3844$ hard spheres of radius $a = 10$ μm in a square box of sidelength $L = 7160$ μm with periodic boundary conditions. The physical parameters were chosen such that $\lambda = 1100$ μm, $\mathcal{K}^{-1} = 49$ μm and $\mathcal{T} = 52863$ s. The Fourier components $\rho_{\mathbf{k}}$ were extracted from the average over 2000 independent runs. The theoretical prediction is represented by the lines. The thin lines represent the case without hydrodynamic interactions, i.e., the solution of the linear equation (1) with $D(k)$ given by Eq. (8), see also Fig. S1. The thick lines correspond to the case that includes hydrodynamic interactions, i.e., with $D(k)$ given by Eq. (2.F).

- In Fig. 2, the tSD simulations employ $N = 50$ particles of radius $a = 5$ μm distributed homogeneously in a disk of initial radius $R = 100$ μm, giving an initial density $\rho_0 \approx (1/7)$ of the 2D close packing density. The disk was placed inside a square box of sidelength $L = 256$ μm with periodic boundary conditions. The physical parameters were chosen such that $\mathcal{K}^{-1} = 26$ μm and $\mathcal{T} = 5935$ s (from Eqs. (4.D, 4.E) with $\rho_{\text{hom}} = \rho_0$), with $\lambda = 1000R = 100000$ μm. The relative mass density of the particles in BD and tSD simulations was set to $\rho_p = 1$. The density profiles were extracted from the average over 10000 independent runs. The parameters of the LB simulations were chosen to match the dynamical regime modelled by the BD and tSD simulations as described in the previous subsection. The density profile was obtained from the average over 30 independent runs containing each $N = 50$ particles. Finally, the dashed lines in Fig. 2 correspond to the theoretical prediction, see Eq. (4.G).

- In Fig. 3, a larger system for the tSD and BD simulations (compared to the setup for Fig. 2) was used ($N = 1804$ particles, radius $a = 10$ μm, initial radius of disk $R = 1832$ μm, initial density $\rho_0 \approx (1/17)$ of the 2D close packing density, $L = 8000$ μm). The physical parameters were chosen such that $\mathcal{K}^{-1} = 34$ μm and $\mathcal{T} = 23835$ s (from Eqs. (4.D, 4.E) with $\rho_{\text{hom}} = \rho_0$), with $\lambda = 0.1R = 183$ μm. The density profiles were extracted from the average over 120 independent runs.

- Fig. 4 shows the results from tSD simulations of an ideal gas of $N = 400$ particles with a hydrodynamic radius $r_H = 10$ μm (i.e., $a = r_H$ only in Eq. (5.B), so that the particles experience hydrodynamic interactions in spite of the absence of a direct interaction). $N_0 = 212$ particles were located in a square box of sidelength $L = 1000$ μm (with periodic boundary conditions), thus giving a background density $\rho_0 = N_0/L^2$. In the initial state, additional $N_d = N - N_0 = 188$ particles were concentrated in a circular patch of radius $R = 100$ μm forming an overdensity $\sim 29\rho_0$. Here, the characteristic time is defined by $\mathcal{T} = (k_B T \Gamma \rho_0)^{-1}$, which corresponds to $\mathcal{T} = 107332$ s for our choice of physical parameters. The density profiles were extracted from the average over 10000 and 50000 independent runs for tSD and BD respectively. The lines correspond to the numerical solution of Eqs. (2–4) with imposed radial symmetry.

References

[1] S. Kim and S. J. Karrila, *Microhydrodynamics: Principles and Selected Applications* (Butterworth–Heinemann, 1991).

[2] G. Batchelor, *J. Fluid Mech.* **52**, 245 (1972).

[3] J. F. Brady, R. J. Phillips, J. C. Lester, and G. Bossis, *J. Fluid Mech.* **195**, 257 (1988).

[4] M. Rex and H. Löwen, *Eur. Phys. J. E* **28**, 139 (2009).

[5] B. U. Felderhof, *Physica A* **153**, 217 (1988).

[6] B. Noetinger, *Physica A* **157**, 1139 (1989).

[7] I. S. Gradshteyn and I. M. Ryzhik, *Table of Integrals, Series, and Products* (Academic Press, 1994).

[8] J. Bleibel, A. Domínguez, M. Oettel, *Eur. Phys. J. Special Topics* **222**, 3071 (2013).

[9] A. Domínguez, M. Oettel, and S. Dietrich, *J. Chem. Phys.* **128**, 114904 (2008).

[10] A. Domínguez, *Capillary Forces between Colloidal Particles at Fluid Interfaces*, in *Structure and Functional Properties of Colloidal Systems*, edited by R. Hidalgo–Alvarez (CRC Press, 2010), p. 31.

[11] A. Domínguez, M. Oettel, and S. Dietrich, *Phys. Rev. E* **82**, 011402 (2010).

[12] J. Bleibel, A. Domínguez, M. Oettel, and S. Dietrich, *Eur. Phys. J. E* **34**, 125 (2011).

[13] J. Bleibel, S. Dietrich, A. Domínguez, and M. Oettel, *Phys. Rev. Lett.* **107**, 128302 (2011).

[14] J. Bleibel, A. Domínguez, M. Oettel, and S. Dietrich, *preprint*, `arxiv:1312.3472 [cond-mat.soft]`.

[15] M. P. Allen and D. J. Tildesley, *Computer Simulation of Liquids* (Oxford University Press, 1987).

[16] J.K.G. Dhont, *An Introduction to Dynamics of Colloids* (Amsterdam, Elsevier, 1996).

[17] F. Jansen and J. Harting, *Phys. Rev. E* **83**, 046707 (2011).

[18] S. Frijters, F. Günther, J. Harting, *Soft Matter* **8**, 6542 (2012).